Macromolecules

pubs.acs.org/Macromolecules Article

Adsorption Kinetics of *cis*-1,4-Polyisoprene in Nanopores by *In Situ* Nanodielectric Spectroscopy

Chien-Hua Tu, Jiajia Zhou, Hans-Juergen Butt, and George Floudas*

Cite This: *Macromolecules* 2021, 54, 6267−6274 Read Online

ACCESS | Metrics & More | Article Recommendations | Supporting Information

ABSTRACT: Using *in situ* nanodielectric spectroscopy, we studied the adsorption kinetics of *cis*-1,4-polyisoprene (PI) into porous alumina by following the evolution of the dielectrically active longest normal mode. We studied the influence of molar mass, nanopore diameter, and surface functionalization. Adsorption times depend strongly on the ratio $2R_g/D$, where R_g is the radius is gyration and D is the pore diameter. For a given pore diameter, the characteristic adsorption times are some 8 orders of magnitude slower than the terminal relaxation times and more than 12 orders of magnitude slower than the segmental times. The extremely slow kinetics reflect the fact that exchanging chains with the pore surface have to pass through several unfavorable configurations (*e.g.*, trains, loops). The molar mass dependence of the characteristic adsorption times ($\tau_{ads} \sim N^{2.6}$) is in good agreement with a scaling theory proposed by de Gennes and later refined by Semenov and Joanny. Subsequently, we investigated the imbibition of miscible PI blends by taking advantage of the difference in imbibition speeds of the respective homopolymers. We show that the shorter chains penetrate first the nanopores, whereas the longer chains enter only at the late stages of the filling process. Moreover, the long-time adsorption is dominated by an exchange mechanism involving primarily the shorter chains. The results from *in situ* nanodielectric spectroscopy demonstrate the capacity of the technique to provide the imbibition length, the adsorption kinetics, and, at the same time, the chain dynamics.

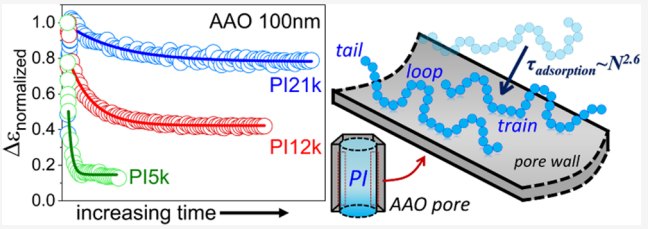

I. INTRODUCTION

There is a growing interest in understanding the way that polymers penetrate narrow pores.[1,2] One example is sequencing DNA with nanopores,[3] a technique based on passing DNA through a nanopore in a membrane and reading off individual bases from the ion current passing through the pore. Another example involving synthetic macromolecules is inkjet printing. In both cases, it is essential to characterize the conformations of the macromolecules inside the pores as well as the polymer−wall interactions.[4−10] The latter is the key factor for the design of polymer interfaces with controlled physical properties (wettability, adhesion, viscosity, glass temperature, etc.) of importance in several applications including membranes, coatings, and organic electronic devices.

In this endeavor, techniques that can provide simultaneous access to the kinetics of imbibition and to the molecular dynamics during and after flow are advantageous. A recent development in this direction has been the implementation of the nanodielectric spectroscopy (*n*DS) technique to follow the imbibition of polymers in nanopores.[11−14] In this technique, a capacitor is formed by the two surfaces of a nanoporous aluminum template and an ac field is applied along the pore axis. A polymer melt on the top surface of a template will penetrate the pores by capillary action. By recording the evolution of capacitance, C, it is possible to extract the complex dielectric permittivity ($C \sim \varepsilon$), where the details of the polymer dynamics during flow (*e.g.*, *in situ*) are encoded. With nanoporous alumina, the probing volumes are typically $\sim 10^{-19}$ m^3 or smaller ($\sim 10^{-20}$ m^3 at the early stages of imbibition) and the polymer mass is $\sim 10^{-15}$ g (*i.e.*, femtograms), hence the term *n*DS. The technique provides simultaneous access to the kinetics of imbibition and to the molecular dynamics during flow at the segmental and chain length scales.

In a recent study,[14] we have employed a type A polymer, *i.e.*, a polymer having components of dipole moment both perpendicular and along the polymer backbone. We could show that interfacial interactions develop already during the polymer flow in nanopores. Herein, we study the adsorption kinetics of *cis*-1,4-polyisoprene as a function of polymer molar mass (M_n = 4840−42 412 g·mol^{-1}), nanopore diameter (100−20 nm), and surface treatment (native vs silanized nanopores) by following the evolution of the longest normal mode. For the confining medium, we employ self-ordered nanoporous aluminum oxide (AAO) that contains arrays of parallel cylindrical nanopores uniform in length (pore depth = 100 μm) and diameter (pore diameters = 100, 40, and 20 nm) that

Received: April 14, 2021
Revised: May 29, 2021
Published: June 18, 2021

https://doi.org/10.1021/acs.macromol.1c00821
Macromolecules 2021, 54, 6267−6274

can easily be infiltrated from the melt.[15] In contrast to the earlier study,[14] here, we are interested in the long-time adsorption kinetics following the full imbibition. The aim is to establish scaling laws for the adsorption time as a function of pore size and molecular mass. We find that adsorption is an extremely slow process because it involves unlocking several unfavorable chain configurations. The characteristic time scale depends strongly on the degree of confinement and molar mass. The experimental findings on the molar mass dependence of the characteristic adsorption times are discussed in view of a scaling theory proposed by De Gennes[4,5] and later refined by Semenov and Joanny.[6]

As an extension of this work, we explore how symmetric PI blends penetrate the same nanopores. This part requires a judicious choice of blend components so that both chains relax within the experimental window at the imbibition temperature. We find that shorter chains (i) penetrate first and (ii) adsorb first on the AAO walls. The longer chains are entering the pores only at the late stages of the filling process, providing an example of polymer fractionation in the absence of solvent. The advantage of *n*DS over other—static—techniques is that it provides the pertinent time scales (chain relaxation) *in situ* and in parallel with the adsorption kinetics.

II. EXPERIMENTAL SECTION

II.I. Samples. Four *cis*-1,4-polyisoprene homopolymers with narrow dispersities, $Đ$, were employed in the present study (Table 1). **PI 12k** and **PI 21k** were purchased from PSS Polymer Standards Service GmbH and used without further purification. **PI 5k** and **PI 42k** were synthesized in house (MPI-P). Two symmetric blends (composition 50/50 wt %) of **PI 5k** with **PI 21k** and of **PI 5k** with **PI 42k** (designated as **B1** and **B2**, respectively) were prepared and investigated in the second part of this study.

Table 1. Molecular Characteristics of the *cis*-1,4-Polyisoprene Homopolymers and Their Blends as Obtained from GPC/SEC

sample	M_n (g·mol^{-1})	M_w (g·mol^{-1})	$Đ$	R_g (nm)[a]	η_o (Pa·s)
PI 5k	4840	5116	1.06	2.3	2.0
PI 12k	11 800	12 000	1.02	3.6	8.8
PI 21k	23 300	23 600	1.01	5.1	
PI 42k	42 412	43 997	1.04	6.9	259.0
B1 (5k/21k)					
B2 (5k/42k)					50.0

[a]The radius of gyration, R_g, was calculated according to $\langle R_g^2\rangle_0 = 1/6\langle R^2\rangle_0$ using $\frac{\langle R^2\rangle_0}{M} = 0.679$ (Å^2 mol/g)).[16]

II.II. AAO Templates. Self-ordered nanoporous aluminum oxide (AAO) templates with both ends open were purchased from InRedox (Longmont). Pore diameters and the corresponding porosities were 100 nm (24 ± 3%), 40 nm (12 ± 2%), and 20 nm (11 ± 2%), respectively, according to the manufacturer, and the pore length was 100 μm. Prior to infiltration, all AAO templates were annealed in a vacuum oven at T = 443 K for 8−10 h. This procedure removes the majority of OH groups from the AAO surface.

II.III. *In Situ* Nanodielectric Spectroscopy. Dielectric spectroscopy (DS) and *in situ* nanodielectric spectroscopy (*n*DS) were employed to follow the dynamics of bulk and confined PI. In both cases, a Novocontrol Alpha frequency analyzer composed of a broadband dielectric converter and an active sample head was used. For bulk samples, polymers were embedded between two stainless steel electrodes with a diameter of 20 mm accompanied with a Teflon spacer of 50 μm to maintain a constant thickness. The sample configuration for *in situ* *n*DS is shown in Figure 1. First, the AAO templates were sputtered with a gold layer (thickness of 35 nm) on both sides. Sputtering was made under vacuum (lower than 2×10^{-5} Pa) by a Bal-tec MED 020 with a current density of 40 mA. The high-vacuum environment is to ensure the uniformity of the sputtered Au layer. The current density during sputtering was optimized to produce Au grains with appropriate size (too big may block the AAO pores; too small may hinder the current transport). Scanning electron microscopy (SEM) was subsequently explored to determine the distribution of Au grains on the inner surface of the AAO templates (Figure 1). In addition to a uniform film deposited on top of the AAO templates, traces of gold are found also within the pores (down to a depth of about 400 nm). However, given the high aspect ratio (>10^3) of nanopores, any inhomogeneities in the field lines can be neglected. A thin film of the polymer was then deposited on the top of the AAO template. For the kinetic studies, the polymer molar mass as well as the temperature and frequency ranges need to be wisely selected. A broad frequency range from 10^{-2} to 10^7 Hz was employed for the bulk DS measurements. In contrast, a narrower frequency range, from 10 to 10^6 Hz, is necessary to probe the imbibition kinetics by *n*DS. With this choice, the time needed for a single dielectric curve is around 2 min. In general, the dielectric function depends on frequency, temperature, and time. At a given time and temperature, it can be fitted by the empirical equation of Havriliak and Negami (HN)[17]

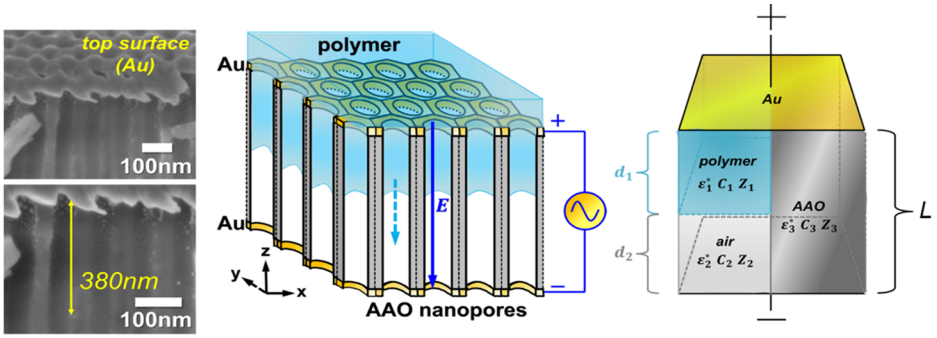

Figure 1. (Left) SEM images showing the top surface and cross section of AAO pores with a diameter of 65 nm after Au sputtering. The left bottom figure is a zoom-in of part of the top image. Au particles are distributed at the top of the nanopores within a distance of 380 nm. (Middle) Schematic of the experimental setup employed for *n*Ds. The blue arrow indicates the direction of the applied electric field, E (along the nanopores, z-axis). The cyan dashed arrow indicates the flow direction of the meniscus within the AAO nanopores. The xyz coordinate represents the laboratory axis. (Right) The equivalent capacitor circuit with Z being the impedance.

https://doi.org/10.1021/acs.macromol.1c00821
Macromolecules 2021, 54, 6267−6274

$$\varepsilon^*_{HN}(\omega, T, t) = \varepsilon_\infty(T, t) + \frac{\Delta\varepsilon(T, t)}{[1 + (i\omega\tau_{HN}(T, t))^{\alpha(t)}]^{\gamma(t)}} + \frac{\sigma_0(T, t)}{i\varepsilon_0\omega} \quad (1)$$

Here, $\Delta\varepsilon(T, t)$ is the relaxation strength, τ_{HN} is the Havriliak–Negami relaxation time, α and γ ($0 < \alpha, \alpha\gamma \leq 1$) are the shape parameters describing the symmetric and asymmetric broadening of dielectric function (with the high-frequency slope in a log–log representation being $\alpha\gamma$), respectively, and ε_∞ is the dielectric permittivity at the limit of high frequencies. At lower frequencies, ε'' increases due to the conductivity ($\varepsilon'' = \sigma_0/(\omega\varepsilon_0)$, where σ_0 is the dc conductivity and ε_0 is the vacuum permittivity). The upturn of ε'' at the higher frequencies is due to the background signal from the Au sputtered electrodes.

II.IV. Simulation of the Imbibition Process. *n*DS provides precise information on the evolution of the imbibition length and the associated polymer dynamics.[11] Modeling the imbibition process requires the use of the equivalent capacitance model (Figure 1). In the parallel model, the capacitance of the polymer (C_1) and air (C_2) are connected in series, whereas the combinational capacitance of the polymer/air (C_{12}) connects in parallel with the capacitance of AAO (C_3). Therefore

$$\frac{1}{C_{12}} = \frac{1}{C_1} + \frac{1}{C_2}, \text{ and } C_{123} = C_{12} + C_3 \quad (2)$$

Since the capacitance is $C = \varepsilon A/L$, where L and A are the thickness and electrode area, respectively, it follows that

$$\varepsilon^*_{12} = \frac{L\varepsilon^*_1}{d_1 + d_2\varepsilon^*_1} \quad (3)$$

$$\varepsilon^*_{123} = \varepsilon^*_{12}\varphi_{12} + \varepsilon^*_3\varphi_3 \quad (4)$$

In the last equation, φ_{12} represents the porosity of AAO templates, $\varphi_3(=1 - \varphi_{12})$ is the AAO area, and L is the full length of the AAO nanopores. After some arrangements, we can obtain the following equation for the complex dielectric permittivity

$$\varepsilon^*_{123} = [\frac{L\varepsilon^*_1}{d_1 + d_2\varepsilon^*_1}]\varphi_{12} + \varepsilon^*_3\varphi_3 \quad (5)$$

Therefore, the imaginary part is

$$\varepsilon''_{123} = \frac{d_1\varepsilon''_1\varphi_{12}}{(d_1 + d_2\varepsilon'_1)^2 + (\varepsilon''_1 d_2)^2} \quad (6)$$

For the real and imaginary parts of the dielectric function of AAO, we employed $\varepsilon_3' = 2.6$ and $\varepsilon_3'' = 0$. The latter value involves the subtraction of the empty cell signal (*e.g.*, the background). Based on eq 6, the presence of an air capacitor can influence the dielectric loss maximum for polar molecules.[18] For nonpolar substances, like PI, the shift of the frequency at the maximum loss during imbibition is insignificant (see Supporting Information Figure S1).

II.V. Calibration Experiments. Independent calibration measurements of the imbibition length were made by employing *ex situ* reflection optical microscopy (ROM). Measurements were made on fractured surfaces of AAO templates and for different imbibition times. Before fracturing, the templates were immersed into liquid nitrogen to prevent the further imbibition of PI into nanopores. For Newtonian liquids, the time dependence of imbibition length, d_1 (Figure 1), can be obtained from the Lucas–Washburn equation (LWE)[19−21]

$$d_1(t) = \left(\frac{\gamma D \cos\theta}{2\eta}\right)^{1/2}\sqrt{t} \quad (7)$$

Here, γ is the surface tension, θ is the advancing contact angle, D is the pore diameter, η is the viscosity, and t is the wetting time. For the surface tension and static contact angle, we have employed the reported values from a PI homopolymer (M_n = 800 g·mol^{-1} and M_w = 880 g·mol^{-1}).[22] The former was measured by the pendant drop method at T = 290 K (γ = 30 mN·m^{-1}), whereas the latter was measured by employing a customized setup on sessile drops at 290 K ($\cos\theta$ = 0.88 ± 0.02). Examples are provided in Supporting Information Figure S2.

II.VI. Rheology. The viscosities of the PI homopolymers and their blends were measured by a shear rheometer (ARES). Measurements were made with the environmental test chamber as a function of temperature ranging from 208.15 to 303.15 K. The zero-shear viscosities at the reference temperature are included in Table 1. Details are provided in the Supporting Information (Figures S3 and S4).

III. RESULTS AND DISCUSSION

III.I. Homopolymer Adsorption. The adsorption kinetics following the full imbibition of *cis*-1,4-polyisoprenes in AAO was studied as a function of pore size and molar mass (Figure 2). Figure 2 depicts the evolution of the dielectric loss curves

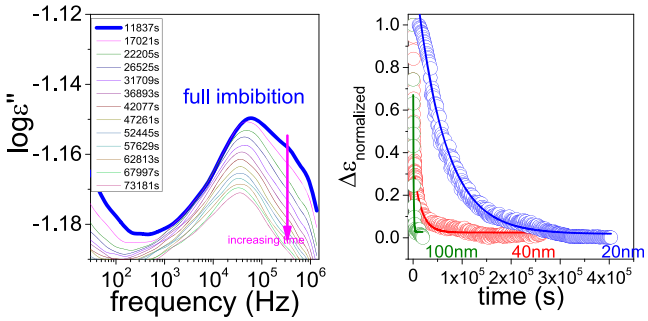

Figure 2. (Left) Evolution of dielectric loss curves at the late stages of imbibition of **PI 5k** within AAO templates having 20 nm diameter pores at T = 303.15 K. (Right) Evolution of the normalized dielectric intensity during the *in situ* imbibition and subsequent adsorption within AAO nanopores with different pore diameters; (green): 100 nm, (red): 40 nm, and (blue): 20 nm all at the same temperature (303.15 K). Lines represent the result of the fit to an exponential decay function (see text).

during and after the full imbibition of **PI 5k** into AAO nanopores having pores with a diameter of 20 nm at 303.15 K. The technique requires a judicious choice of the parameters (temperature/molar mass) such that the spectrum of normal modes is contributing to the dielectric loss within the investigated (restricted) frequency window at the imbibition temperature. At this temperature, the segmental dynamics are out of the accessible frequency window. We observed increasing dielectric loss curves for the longest normal mode during imbibition until after 12 000 s when the trend reversed and the dielectric loss curves start to decrease in intensity. The same figure compiles the evolution in the dielectric strength, $\Delta\varepsilon$, of the normal mode for the same PI following imbibition in AAO with different pore diameters. This trend is more evident in the smaller pores. Note the very long time scales, in the case of the 20 nm pores, in the order of (several) days. We will return to this point below.

In Figure 2, the dielectric strength is normalized to the maximum value. The maximum, $\Delta\varepsilon_n$, coincides with the full imbibition of the polymer as evidenced by independent measurements by reflection optical microscopy (ROM). At subsequent times, the strength of the normal mode is decreasing due to increasing adsorption. In the figure, the dielectric strength is normalized (from max (1) to min (0) values) to make the comparison of the time scales more

https://doi.org/10.1021/acs.macromol.1c00821
Macromolecules 2021, 54, 6267−6274

evident. Polymer adsorption gives rise to train and loop chain configurations that are dielectrically inactive because part of the chain cannot fluctuate in space and time. This is evident, as the dielectric strength for the normal mode is given by[23−32]

$$\Delta\varepsilon = \frac{N_A \mu_{NM}^2}{3\varepsilon_0 k_B T}\frac{\langle r^2\rangle}{M_{PI}} \quad (8)$$

Here, $\langle r^2\rangle$ is the mean-square end-to-end distance, μ_{NM} is the dipole moment per contour length, and M_{PI} is the chain molar mass. The decrease in dielectric strength can be parameterized by an exponential function as $\Delta\varepsilon = \Delta\varepsilon_{max}\ (\exp^{-t/\tau_{ads}})$, where τ_{ads} is the characteristic adsorption time. A single exponential is the simplest approach to describe the desorption process as rate-limited by the energetics of surface detachment.[33] At the same time, we can record the position (frequency of maximum loss, f_{max}) of the normal mode, that relates to the longest relaxation time as $\tau_{max} = 1/(2\pi f_{max})$. Hence, *n*DS provides simultaneous access to the adsorption kinetics and to the chain dynamics during adsorption.

The results of the adsorption kinetics of **PI 5k** can be discussed with the help of Figure 3. The figure depicts the

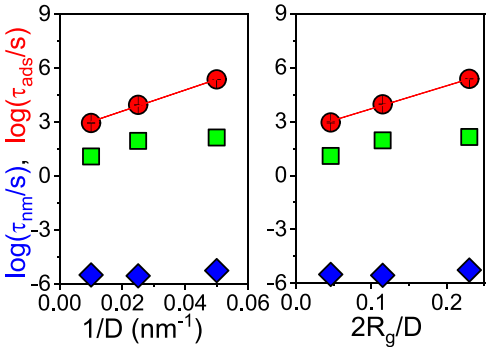

Figure 3. Dependence of the characteristic adsorption time $\log(\tau_{ads}/s)$ on (left) the inverse pore diameter and (right) the degree of confinement, defined by the ratio of polymer size ($2R_g$) to the pore diameter for **PI 5k**: (red spheres): characteristic adsorption times obtained from the fits shown in Figure 2. The lines represent the result of a linear fit. The time scale of the longest normal mode (blue solid rhombi) is also plotted at the end of the adsorption process (see Figure S5). The time of full imbibition is plotted with the green solid squares. Error bars give the uncertainties (typically smaller than the symbol size).

characteristic adsorption time, $\log(\tau_{ads}/s)$ as a function of the inverse pore diameter (Figure 3a) and as a function of the degree of confinement (Figure 3b), the latter defined by the ratio of the polymer coil size ($2R_g$) to the pore diameter. In addition, the figure contains the time required for the full imbibition of the pores (in green) extracted by ROM (this time coincides with the $\Delta\varepsilon_{max}$). The adsorption time follows the dependencies as: $\log(\tau_{ads}/s) = 2.2 \pm 0.2 + \frac{62\pm 8}{D}$, ($D$ in nm) and $\log(\tau_{ads}/s) = 2.2 \pm 0.2 + (13.5\pm1.8) \times \frac{2R_g}{D}$, ($D$ in nm), *e.g.*, strongly increasing with confinement. The characteristic relaxation times of the longest normal mode obtained from the dielectric loss maximum at the end of the imbibition process are also shown. Notably, this time scale is somewhat longer than in the bulk especially within the smaller pores (Supporting Information Figure S5). This finding could reflect an increasing density of topological constraints as a result of the loop/train configurations of the adsorbed chains. Loop/train configurations are expected to reduce the critical molecular weight for entanglements for chains in the vicinity to the pore walls. The results presented here as well as in ref 11 are consistent with the notion of surface-enhanced entanglements that "propagate" in the direction normal to the surface.[34] On the other hand, the results on the time scale of chain relaxation obtained *in situ* by following the full imbibition are at variance from earlier results on 3-d as well as 1-d and 2-d confined PI that reported faster chain dynamics through the relaxation of terminal subchains.[27,35]

A direct proof that the decrease in the dielectric intensity of the longest normal mode is due to the adsorption of chains is provided by following the same kinetics but in a treated (silanized) AAO surface. The results between untreated and treated surfaces for a **PI 21k** within AAO templates having pores with a diameter of 100 nm at 303.15 K are compared in Figure 4. Following the full imbibition, the dielectric strength

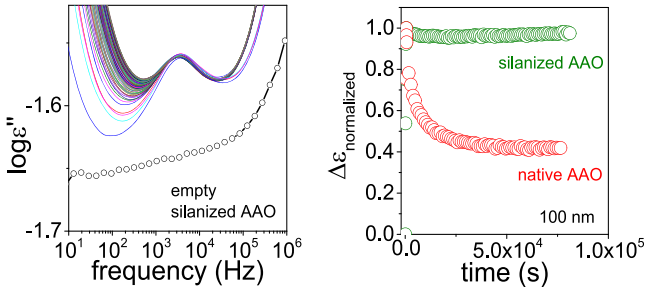

Figure 4. (a) Evolution of the dielectric loss curves during and following the complete imbibition of **PI 12k** within silanized AAO nanopores having pore diameters of 100 nm at T = 303.15 K. (b) Evolution of dielectric intensity ($\Delta\varepsilon$) of **PI 12k** during the *in situ* imbibition (and subsequent adsorption) within nanopores with a native (red) or silanized (green) inner pore surface.

in a silanized pore remains constant with time in sharp contrast to the native AAO surface. Evidently, silanization is very effective in reducing adsorption sites acting as a lubricant for the incoming chains.

Next, we discuss the evolution of the distribution of relaxation times during and following polymer imbibition. The data refer to **PI 21k**, where the maximum in the loss of the chain modes is well within the frequency window. In Figure 5, the evolution of the dielectric loss curves at the late stages of imbibition within AAO templates having 40 nm pores at

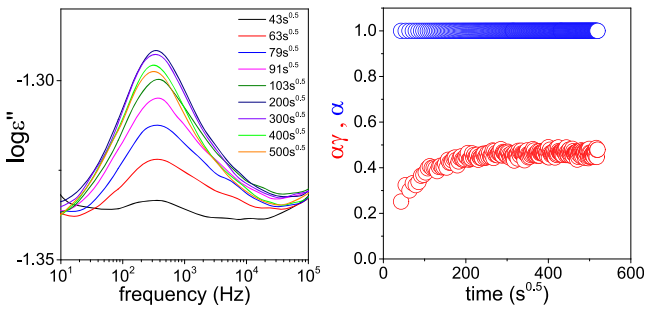

Figure 5. (Left) Evolution of the dielectric loss curves at the late stages of imbibition of **PI 21k** within AAO templates having 40 nm pores at 303.15 K. (Right) Evolution of the HN shape parameters.

https://doi.org/10.1021/acs.macromol.1c00821
Macromolecules 2021, 54, 6267−6274

303.15 K are shown. The same figure depicts the low- and high-frequency HN parameters during the adsorption kinetics. The evolution of the high-frequency slope ($\alpha\gamma$) shows the narrowing of the distribution of relaxation times with time. The broader distribution at the earlier stages reflects the continuous changes due to chain adsorption.

The chain length dependence of the adsorption process is examined next. Figure 6 provides the evolution of dielectric

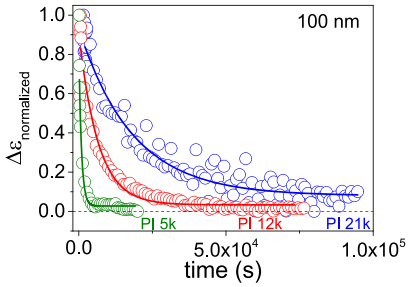

Figure 6. Evolution of dielectric intensity ($\Delta\varepsilon$) of **PI** with different molar masses during the *in situ* imbibition (and subsequent adsorption) within AAO nanopores with a diameter of 100 nm at a temperature of 303.15 K. Lines represent fits to an exponential decay function.

strength for three PIs with molar masses of 5, 12, and 21 kg·mol^{-1} within AAO templates with a pore size of 100 nm at 303.15 K. The normalized dielectric strength was again fitted to an exponential function, and the characteristic adsorption times are plotted in Figure 6. Evidently, adsorption times become much longer with increasing molar mass. Additional data for a smaller pore diameter (40 nm) are provided in Supporting Information Figure S6.

The different time scales can be discussed with the help of Figure 7. The figure contains in total four time scales: The faster (~*ns*) is the segmental relaxation obtained from the Vogel–Fulcher–Tammann (VFT) equation at the imbibition temperature (303.15 K) (Supporting Information Figure S7).

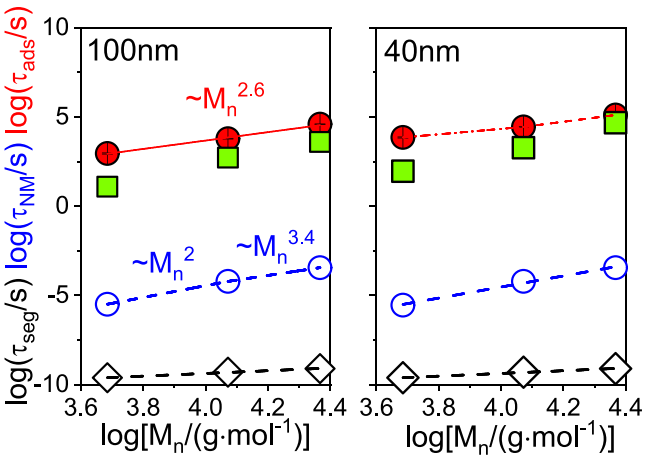

Figure 7. Molar mass dependence of the characteristic time scales within AAO nanopores with pore diameters (left) 100 nm and (right) 40 nm; (green squares): full imbibition time, (red spheres): characteristic adsorption time following imbibition, (blue solid/empty circles): peak position of the longest normal mode of polyisoprene under confinement (at the end of adsorption process). Dashed and dash-dotted lines are linear fits. Error bars give the uncertainties (typically smaller than the symbol size).

The latter was obtained immediately following the kinetic experiments by fast cooling to below T_g and slow heating to higher temperatures. As expected, this time scale is the fastest without a significant dependence on molar mass. The second time scale is the longest normal mode obtained at the end of the imbibition process as $\tau_{max} = 1/(2\pi f_{max})$ (Supporting Information Figure S5). The critical molar mass M_c for PI is ~10 800 g·mol^{-1} (the entanglement molecular weight is M_e ~ 5400 g·mol^{-1}) meaning that **PI 5k** is unentangled, **PI 21k** is entangled, and **PI 12k** is in the border region.[16] Despite the limited data points two slopes can be obtained with exponents of approximately 2 and 3.4 below and above M_c. The third time scale corresponds to the time needed for the full imbibition and has a clear molar mass dependence. Finally, the fourth time scale reflects the adsorption times that strongly depend on both the molar mass and the pore size. Adsorption times are (i) some 8 orders of magnitude slower than the terminal relaxation times (*e.g.*, the relaxation of the chain as a whole) and (ii) display a similar molar mass dependence with the terminal times. Interestingly, annealing times were also found to scale with the chain relaxation times in confined poly(propylene glycol) within AAO templates (although through a different temperature protocol).[36,37]

The very long time scale of adsorption can be discussed in view of a scaling theory developed by De Gennes[4,5] that accounts for the formation of adsorbed layers in a good solvent. At early stages, a uniform polymer layer was considered on the (flat) surface as a result of bulk diffusion. Subsequent formation of an adsorbed layer was considered as a two-step process. At a first step, any new chain to be adsorbed needs to overcome the potential barrier due to the excluded volume of the already adsorbed chains. At a second step, the incoming chain replaces the already adsorbed chains by spreading on the surface, whereas the previously adsorbed chain unfolds by the formation of long loops. As outgoing (and incoming) chains have to pass through several unfavorable configurations the latter process was predicted to be very slow. As for the molar mass dependence, by considering entangled polymers, de Gennes suggested that the longest relaxation time scales as $\tau \sim \tau_s N^3$, where τ_s is the relaxation time of an adsorbed monomer. Subsequently, Semenov and Joanny[6] considered explicitly the structure of tails and loops within the adsorbed layer (the chain ends are effectively repelled from the surface) and further assumed Rouse-Zimm dynamics to predict the molar mass dependence of two characteristic times scales, the adsorption and the exchange times, with respective scaling as $\tau \sim N^{2.24}$ and $N^{2.42}$. Both of these dependencies are in line with the experimental results over the limited range of molar masses investigated. Extending the range of molar masses is a formidable task due to limitations associated with the experimental frequency window and imbibition temperature.

III.II. Blend Imbibition and Adsorption. We further investigated the effect of blending on the imbibition and adsorption kinetics for two symmetric PI blends (**B1** (5/21k) and **B2** (5/42k)). While the short chains do not entangle, the long chains are above the entanglement limit.[16] The question is whether the two components penetrate and adsorb on the pores simultaneously or consecutively. We mention here that earlier experiments using *ex situ* methods have demonstrated the ability of the AAO templates to effectively separate the components of miscible blends by taking advantage of the difference in the imbibition speeds of the respective

https://doi.org/10.1021/acs.macromol.1c00821
Macromolecules 2021, 54, 6267–6274

homopolymers.[38,39] These techniques, however, have two shortcomings: First, they do not provide the respective time scales, and second, they cannot follow the adsorption kinetics. The advantage of nanodielectric spectroscopy is that it simultaneously provides access to the imbibition length and the adsorption kinetics by following the change in the dielectric strength of the chain relaxation.

The results for blend **B2** with respect to the evolution of the dielectric loss curves during and following the full imbibition are shown in Figure 8. The evolution of the dielectric loss

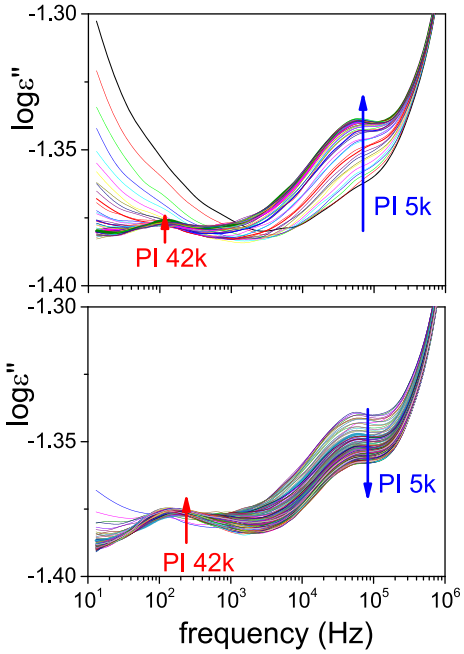

Figure 8. Evolution of dielectric loss curves corresponding to the two separate normal modes of PI in blend **B2** (5/42k) during imbibition and subsequent long-time adsorption within AAO with a pore diameter of 40 nm at 303.15 K. Early (top) and late (below) stages are shown. Arrows are indicative trends for the evolution of the dielectric loss curves corresponding to the normal modes of **PI 5k** (blue) and **PI 42k** (red) components in the blend.

curves corresponding to the shorter and longer chains in the blend reveals distinct differences that will be discussed below with respect to Figure 10. We should point out here that the choice of the blend components in **B1** and **B2** is based on the existence of two separate normal modes in the blends both relaxing within the experimental window: a slower (faster) one reflecting the dynamics of the longer (shorter) chains in the blend. We will first discuss the results from blend **B1**.

The evolution of the dielectric intensities of the two separate normal modes in blend **B1** is provided in Figure 9. We point out that in the blend there exists a single local friction as obtained by temperature-dependent measurements of the (single) segmental process in the blends. The results are compared to independent ROM measurements of the imbibition length in comparison to the respective homopolymers (Figure 9b). The imbibition lengths for blend **B1** are located in between the corresponding lengths for the two homopolymers. It further suggests the complete imbibition of the blend in ~620 s. At this time, the increase of the dielectric strength of the normal mode for the **PI 5k** component in the blend reaches a maximum. Following the full imbibition, the

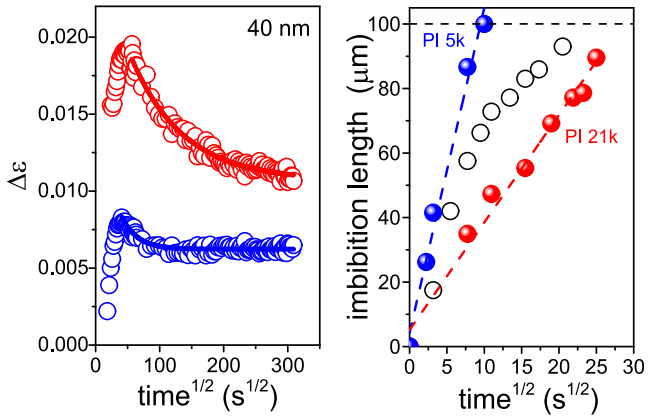

Figure 9. (Left) Evolution of dielectric intensity for the PI blend **B1** (5/21k) during imbibition and subsequent long adsorption within AAO with a pore diameter of 40 nm at T = 303.15 K. (Right) Imbibition lengths measured *ex situ* by ROM for three systems: homopolymer **PI 5k** (blue spheres), homopolymer **PI 21k** (red spheres), and **B1** blend (black circles). Blue and red dashed lines represent linear fits to the homopolymer data. The horizontal dashed line indicates the length corresponding to full imbibition.

dielectric strength of the **PI 5k** component decreases due to adsorption with a characteristic adsorption time of ~2.9×10^3 s. The evolution of the dielectric strength of the **PI 21k** bears similarities to the lower-molecular-weight component albeit with one difference. The maximum dielectric strength is attained somewhat later, and the characteristic adsorption time increases to 1.5×10^4 s. The latter is in agreement with the characteristic adsorption times of the respective homopolymers discussed with respect to Figure 6. This suggests that in blend **B1**, imbibition of the two components proceeds with somewhat different rates; first, the shorter chains are entering the nanopores, and somewhat later, the longer chains penetrate together with the remaining short chains. The difference in imbibition speeds, however, is not dramatic. To enhance the difference in imbibition speeds of the two components, we return to blend **B2** (**5/42k**) (Figures 8 and 10).

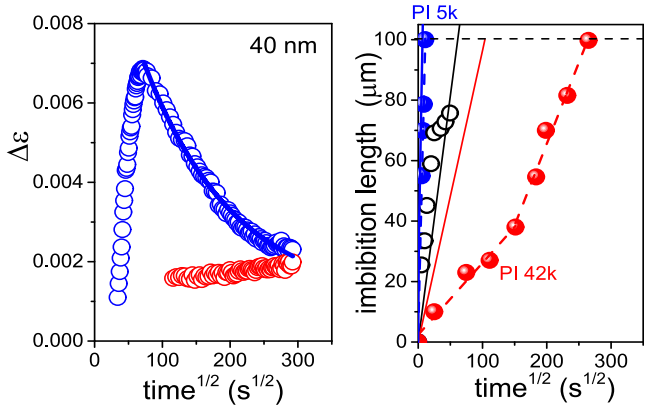

Figure 10. (Left) Evolution of dielectric intensity for the PI blend **B2** (5/42k) during imbibition and subsequent long adsorption within AAO with a pore diameter of 40 nm at T = 303.15 K. (Right) Imbibition length measured *ex situ* by ROM for three systems: homopolymer **PI 5k** (blue spheres), homopolymer **PI 42k** (red spheres), and **B2** blend (black circles). Blue, red, and black solid lines are the predictions of the imbibition length based on the LWE and the measured zero-shear viscosity (Table 1).

https://doi.org/10.1021/acs.macromol.1c00821
Macromolecules 2021, 54, 6267−6274

The results of blend **B2** (Figure 10) are distinctly different from those of **B1**. This is evident here as the blend components have very different imbibition speeds. Note that the imbibition lengths of the homopolymers calculated from the LWE based on the measured (Table 1) zero-shear viscosities (solid lines in Figure 10b) are at variance from the measured lengths. While for the homopolymer **PI 5k** the extracted effective viscosity from the imbibition length and the use of the LWE is approximately the bulk zero-shear viscosity, for the **PI 42k** homopolymer there exist two slopes during imbibition with effective viscosities of 4660 and 910 Pa·s, *e.g.*, much higher than bulk (Table 1). This finding reveals that the dead-layer effect is dominant.[11] For the blend, the results from the ROM study (Figure 10b) suggest that the imbibition length, d_1, is in proximity to the **PI 5k** homopolymer revealing a clear preference for the shorter chains to penetrate the pores. The emerging picture from these results is that the **PI 5k** chains enter first, and only later, some **PI 42k** are dragged into the pores. This is more evident here because the two homopolymers have very different imbibition speeds.

These results on the "static" imbibition length obtained *ex situ* (ROM) can be compared with the results from dynamic experiment performed *in situ* (*n*DS). In accordance with the static measurement revealing the faster imbibition of the shorter chains, the dielectric strength of the **PI 5k** blend component (Figures 8 and 10a) first increases during imbibition and reaches a maximum at a time scale that nicely corresponds to the full imbibition (as obtained from ROM). It is only at the late stages of the pore filling that the shorter chains drag along some of the longer chains in the pores as evidenced by the slow increase in the dielectric strength of the **PI 42k** component. At the same time, the normal mode of the **PI 5k** blend component starts to decrease as a result of increasing adsorption. Hence, at the late stages of imbibition, two effects take place: first, the shorter chains are adsorbed onto the AAO pore surface, and at the same time, some of the longer chains are entering the pores. This further suggests that long-time adsorption in the blend is dominated by an exchange mechanism involving primarily the shorter chains.

Overall, results show an efficient separation of long/short chains in a miscible polymer blend by following the imbibition length and the associated dynamics of the longest normal modes. Although previous techniques[11,38,39] were able to show the potential of AAO templates in separating chains of different molar masses and in the absence of solvent, *n*DS has the advantage of providing the chain dynamics at the same time. When the blend components have drastically different molar masses (M_n(long)/M_n(short) ~8) the long-time adsorption kinetics is dominated by the shorter chains, otherwise (*i.e.*, M_n(long)/M_n(short) ~4) both chains participate in the adsorption process.

IV. CONCLUSIONS

The adsorption kinetics of *cis*-1,4-polyisoprene was studied as a function of polymer molar mass, AAO pore diameter, and surface treatment by following the evolution of the dielectrically active longest normal mode by nanodielectric spectroscopy. Following the initial imbibition of polymer chains and the formation of an adsorbed layer, the adsorption of other chains is an extremely slow process. For a given molar mass, the characteristic adsorption times strongly depend on the ratio $2R_g/D$. For a given pore diameter, adsorption times are some 8 orders of magnitude slower than the terminal relaxation times and more than 12 orders of magnitude slower than the segmental times. Nevertheless, the adsorption and terminal relaxation times display similar molar mass dependences. The extremely slow kinetics reflect the fact that incoming and outgoing chains from the pore surface have to pass through several unfavorable configurations (*e.g.*, trains, loops). The molar mass dependence of the characteristic adsorption times is in good agreement with a scaling theory proposed by de Gennes and later refined by Semenov and Joanny, to account explicitly the structure of tails and loops within the adsorbed layer. The latter suggested that the adsorption and exchange times scale as $\tau \sim N^{2.24}$ and $N^{2.42}$ not far from the experimental observations given the small molar mass range accessible by *n*DS.

As an extension of this work, we explored how symmetric PI blends penetrate the same nanopores. Of particular interest were blends where the imbibition speeds of the two homopolymers were very different. By taking advantage of the disparity in the imbibition speeds, we were able to show that shorter chains penetrate first and, in addition, that they adsorb first on the AAO walls. The longer chains are entering the pores only at the late stages of the filling process providing an example of fractionation and in the absence of solvent. The results from *n*DS demonstrate the advantage of the technique to provide the imbibition lengths, adsorption kinetics, and chain dynamics.

In a broader context, the results suggest means of controlling the interfacial interactions in homopolymers and their blends of importance in the design of polymer interfaces with controlled physical processes.

■ ASSOCIATED CONTENT

Supporting Information

The Supporting Information is available free of charge at https://pubs.acs.org/doi/10.1021/acs.macromol.1c00821.

Simulation of the imbibition process, bulk rheology data, and additional dielectric data (PDF)

■ AUTHOR INFORMATION

Corresponding Author

George Floudas − *Max Planck Institute for Polymer Research, 55128 Mainz, Germany; Department of Physics, University of Ioannina, 45110 Ioannina, Greece; Institute of Materials Science and Computing, University Research Center of Ioannina (URCI), 45110 Ioannina, Greece;* orcid.org/0000-0003-4629-3817; Email: gfloudas@uoi.gr

Authors

Chien-Hua Tu − *Max Planck Institute for Polymer Research, 55128 Mainz, Germany*

Jiajia Zhou − *South China Advanced Institute for Soft Matter Science and Technology, School of Molecular Science and Engineering, South China University of Technology, Guangzhou 510640, China;* orcid.org/0000-0002-2258-6757

Hans-Juergen Butt − *Max Planck Institute for Polymer Research, 55128 Mainz, Germany;* orcid.org/0000-0001-5391-2618

Complete contact information is available at: https://pubs.acs.org/10.1021/acs.macromol.1c00821

https://doi.org/10.1021/acs.macromol.1c00821
Macromolecules 2021, 54, 6267−6274

Notes

The authors declare no competing financial interest.

■ ACKNOWLEDGMENTS

This research was supported by the Hellenic Foundation for Research and Innovation (H.F.R.I.) under the "First Call for H.F.R.I. Research Projects to support Faculty members and Researchers and the procurement of high-cost research equipment grant" (Project Number: 183).

■ REFERENCES

(1) De Gennes, P. G. Scaling Theory of Polymer Adsorption. *J. Phys.* **1976**, *37*, 1445−1452.
(2) Granick, S. Motions and Relaxations of Confined Liquids. *Science* **1991**, *253*, 1374−1379.
(3) Aksimentiev, A.; Heng, J. B.; Timp, G.; Schulten, K. Microscopic Kinetics of DNA Translocation through Synthetic Nanopores. *Biophys. J.* **2004**, *87*, 2086−2097.
(4) De Gennes, P. G. Polymer Solutions near an Interface. Adsorption and Depletion Layers. *Macromolecules* **1981**, *14*, 1637−1644.
(5) de Gennes, P. G. Polymers at an Interface; a Simplified View. *Adv. Colloid Interface Sci.* **1987**, *27*, 189−209.
(6) Semenov, A. N.; Joanny, J.-F. Kinetics of Adsorption of Linear Homopolymers onto Flat Surfaces: Rouse Dynamics. *J. Phys. II* **1995**, *5*, 859−876.
(7) O'Shaughnessy, B.; Vavylonis, D. Non-equilibrium in Adsorbed Polymer Layers. *J. Phys.: Condens. Matter* **2004**, *17*, R63−R99.
(8) Ligoure, C.; Leibler, L. Thermodynamics and Kinetics of Grafting End-functionalized Polymers to an Interface. *J. Phys.* **1990**, *51*, 1313−1328.
(9) *Dynamics in Geometrical Confinement*; Kremer, F., Ed.; Springer: Berlin, 2014.
(10) Napolitano, S.; Wübbenhorst, M. The Lifetime of the Deviations from Bulk Behaviour in Polymers Confined at the Nanoscale. *Nat. Commun.* **2011**, *2*, No. 260.
(11) Tu, C.-H.; Steinhart, M.; Butt, H.-J.; Floudas, G. In Situ Monitoring of the Imbibition of Poly (*n*-butyl methacrylates) in Nanoporous Alumina by Dielectric Spectroscopy. *Macromolecules* **2019**, *52*, 8167−8176.
(12) Serghei, A.; Chen, D.; Lee, D. H.; Russell, T. P. Segmental Dynamics of Polymers during Capillary Flow into Nanopores. *Soft Matter* **2010**, *6*, 1111−1113.
(13) Serghei, A.; Lutkenhaus, J. L.; Miranda, D. F.; McEnnis, K.; Kremer, F.; Russell, T. P. Density Fluctuations and Phase Transitions of Ferroelectric Polymer Nanowires. *Small* **2010**, *6*, 1822−1826.
(14) Tu, C.-H.; Zhou, J.; Doi, M.; Butt, H.-J.; Floudas, G. Interfacial Interactions During In Situ Polymer Imbibition in Nanopores. *Phys. Rev. Lett.* **2020**, *125*, No. 127802.
(15) Masuda, H.; Fukuda, K. Ordered Metal Nanohole Arrays Made by a Two-step Replication of Honeycomb Structures of Anodic Alumina. *Science* **1995**, *268*, 1466−1468.
(16) Fetters, L. J.; Lohse, D. J.; Colby, R. H. Chain Dimensions and Entanglement Spacings. In *Physical Properties of Polymers Handbook*; Springer: New York, NY, 2007; pp 447−454.
(17) *Broadband Dielectric Spectroscopy*; Kremer, F.; Schönhals, A., Eds.; Springer Science & Business Media, 2002.
(18) Tu, C-.H.; Steinhart, M.; Butt, H-J.; Floudas, G. Polymers under 2-D Confinement: Flow of Polymer Melts at the Nanoscale. In *Broadband Dielectric Spectroscopy: A Modern Analytical Technique*; American Chemical Society, 2021; pp 203−221.
(19) Lucas, R. Ueber das Zeitgesetz des Kapillaren Aufstiegs von Flüssigkeiten. *Kolloid-Zeitschrift* **1918**, *23*, 15−22.
(20) Washburn, E. W. The Dynamics of Capillary Flow. *Phys. Rev.* **1921**, *17*, 273−283.
(21) Yao, Y.; Alexandris, S.; Henrich, F.; Auernhammer, G.; Steinhart, M.; Butt, H.-J.; Floudas, G. Complex Dynamics of Capillary Imbibition of Poly(ethylene oxide) Melts in Nanoporous Alumina. *J. Chem. Phys.* **2017**, *146*, No. 203320.
(22) Alexandris, S.; Papadopoulos, P.; Sakellariou, G.; Steinhart, M.; Butt, H.-J.; Floudas, G. Interfacial Energy and Glass Temperature of Polymers Confined to Nanoporous Alumina. *Macromolecules* **2016**, *49*, 7400−7414.
(23) Adachi, K.; Kotaka, T. Dielectric Normal Mode Process in Undiluted Cis-polyisoprene. *Macromolecules* **1985**, *18*, 466−472.
(24) Boese, D.; Kremer, F.; Fetters, L. J. Molecular Dynamics in Linear and Multiarmed Star Polymers of Cis-polyisoprene as Studied by Dielectric Spectroscopy. *Macromolecules* **1990**, *23*, 1826−1830.
(25) Schoenhals, A. Relation between Main and Normal Mode Relaxations for Polyisoprene Studied by Dielectric Spectroscopy. *Macromolecules* **1993**, *26*, 1309−1312.
(26) Floudas, G.; Paraskeva, S.; Hadjichristidis, N.; Fytas, G.; Chu, B.; Semenov, A. N. Dynamics of Polyisoprene in Star Block Copolymers Confined in Microstructures: A Dielectric Spectroscopy Study. *J. Chem. Phys.* **1997**, *107*, 5502−5509.
(27) Petychakis, L.; Floudas, G.; Fleischer, G. Chain Dynamics of Polyisoprene Confined in Porous Media. A Dielectric Spectroscopy Study. *Europys. Lett.* **1997**, *40*, 685.
(28) Alexandris, S.; Sakellariou, G.; Steinhart, M.; Floudas, G. Dynamics of Unentangled Cis-1,4-polyisoprene Confined to Nanoporous Alumina. *Macromolecules* **2014**, *47*, 3895−3900.
(29) Tarnacka, M.; Kaminski, K.; Mapesa, E. U.; Kaminska, E.; Paluch, M. Studies on the Temperature and Time Induced Variation in the Segmental and Chain Dynamics in Poly (propylene glycol) Confined at the Nanoscale. *Macromolecules* **2016**, *49*, 6678−6686.
(30) Talik, A.; Tarnacka, M.; Grudzka-Flak, I.; Maksym, P.; Geppert-Rybczynska, M.; Wolnica, K.; Kaminska, E.; Kaminski, K.; Paluch, M. The Role of Interfacial Energy and Specific Interactions on the Behavior of Poly (propylene glycol) Derivatives under 2D Confinement. *Macromolecules* **2018**, *51*, 4840−4852.
(31) Politidis, C.; Alexandris, S.; Sakellariou, G.; Steinhart, M.; Floudas, G. Dynamics of Entangled Cis-1, 4-polyisoprene Confined to Nanoporous Alumina. *Macromolecules* **2019**, *52*, 4185−4195.
(32) Watanabe, H.; Ishida, S.; Matsumiya, Y. Rheodielectric Behavior of Entangled Cis-polyisoprene under Fast Shear. *Macromolecules* **2002**, *35*, 8802−8818.
(33) Douglas, J. F.; Johnson, H. E.; Granick, S. A Simple Kinetic Model of Polymer Adsorption and Desorption. *Science* **1993**, *262*, 2010−2012.
(34) Granick, S. Perspective: Kinetic and Mechanical Properties of Adsorbed Polymer Layers. *Eur. Phys. J.E.* **2002**, *9*, 421−424.
(35) Mapesa, E. U.; Popp, L.; Kipnusu, W. K.; Tress, M.; Kremer, M. Molecular Dynamics in 1- and 2-D Confinement as Studied for the Case of Poly(Cis-1,4-Isoprene). *Soft Materials* **2014**, *12*, S22−S30.
(36) Tarnacka, M.; Talik, A.; Kaminska, E.; Geppert-Rybczynska, M.; Kaminski, K.; Paluch, M. The Impact of Molecular Weight on the Behavior of Poly(propylene glycol) Derivatives Confined within Alumina Templates. *Macromolecules* **2019**, *52*, 3516−3529.
(37) Tarnacka, M.; Olga Madejczyk, O.; Kaminski, K.; Paluch, M. Time and Temperature as Key Parameters Controlling Dynamics and Properties of Spatially Restricted Polymers. *Macromolecules* **2017**, *50*, 5188−5193.
(38) Yao, Y.; Butt, H.-J.; Zhou, J.; Doi, M.; Floudas, G. Capillary Imbibition of Polymer Mixtures in Nanopores. *Macromolecules* **2018**, *51*, 3059−3065.
(39) Zhang, M.; Dobriyal, P.; Chen, J. T.; Russell, T. P.; Olmo, J.; Merry, A. Wetting Transition in Cylindrical Alumina Nanopores with Polymer Melts. *Nano Lett.* **2006**, *6*, 1075−1079.

https://doi.org/10.1021/acs.macromol.1c00821
Macromolecules 2021, 54, 6267−6274

Supporting Information

Adsorption Kinetics of *cis*-1,4-Polyisoprene in Nanopores by *In Situ* Nanodielectric Spectroscopy

Chien-Hua Tu,[1] Jiajia Zhou,[2] Hans-Juergen Butt,[1] and George Floudas[1,3,4*]

[1] *Max Planck Institute for Polymer Research, 55128 Mainz, Germany*

[2] *South China Advanced Institute for Soft Matter Science and Technology, School of Molecular Science and Engineering, South China University of Technology, Guangzhou, China*

[3] *Department of Physics, University of Ioannina, 45110 Ioannina, Greece*

[4] *University Research Center of Ioannina (URCI) - Institute of Materials Science and Computing, 45110 Ioannina, Greece*

**Corresponding author: gfloudas@uoi.gr*

I. Simulation of the imbibition process of PI

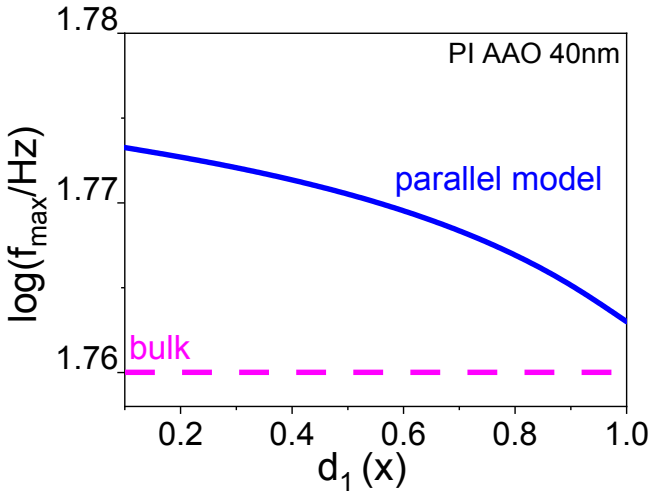

Figure S1. Evolution of the peak frequency for the non-polar polymer PI during imbibition as a function of polymer penetration depth, d_1, based on the parallel model.

II. Calibration experiments (Reflection Optical Microscopy)

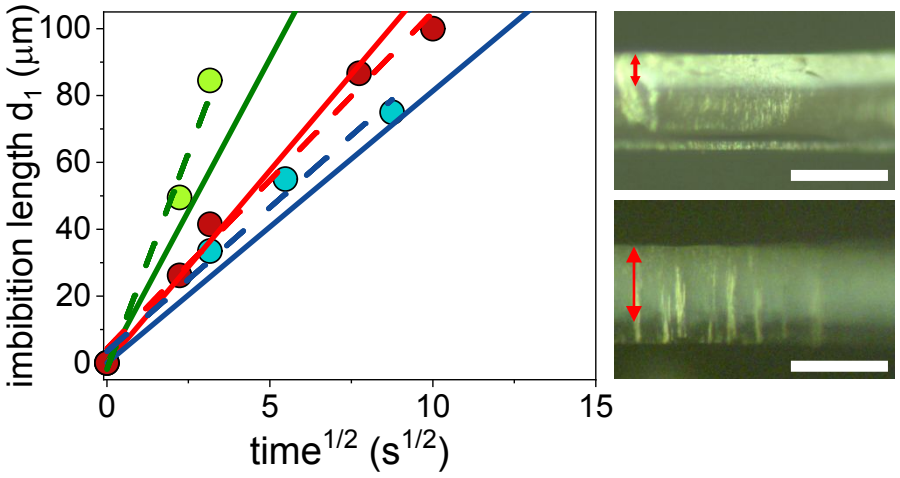

Figure S2. (Left) Calibration measurements for the imbibition of **PI 5k** within different AAO pores: 100 nm (green), 40 nm (red), and 20 nm (blue). Dashed lines are linear fits. Solid lines are theoretical predictions according to Lucas-Washburn equation with bulk viscosity. (Right) Representative ROM images obtained *ex situ* during the imbibition of **PI 5k** within AAO 20 nm at 303 K corresponding to different time periods: (top) $3.16 s^{1/2}$ and (bottom) $8.7 s^{1/2}$. The scale bar is 100 μm.

III. Rheology

Samples were prepared on the lower plate of the 8 and 25 mm diameter parallel plate geometry. The upper plate was brought into contact, the gap thickness was adjusted and the sample was cooled. The storage (G') and loss (G'') shear moduli were monitored as a function of frequency, ω, for frequencies in the range from $10^{-2}<\omega<10^{2}$ rad/s. All measurements refer to the linear viscoelastic range. Subsequently, the complex viscosity (η^*) follows as $\eta^* = G''/\omega - iG'/\omega$. Master curves at the same reference temperature (the imbibition temperature, T=303.15 K) were made by using the time-temperature superposition principle (tTs). The latter allows the frequency ω dependence of the complex modulus G^* at any temperature T to be determined from a master curve at a reference temperature. At each temperature T, a single frequency-scale shift factor a_T allow superposition of all viscoelastic data at temperature T with the data at the reference temperature, T_{ref}, as: $G^*(\omega;T) = G^*(a_T\omega;T_{ref})$. Master-curves of the storage, the loss moduli and the shear viscosity are shown in **Figure S3** all at the same reference temperature of 303.15 K. The shift factors a_T and Williams-Landel-Ferry (WLF) coefficients (C_1^0, C_2^0 at T_{ref}) are shown in **Figure S4**.

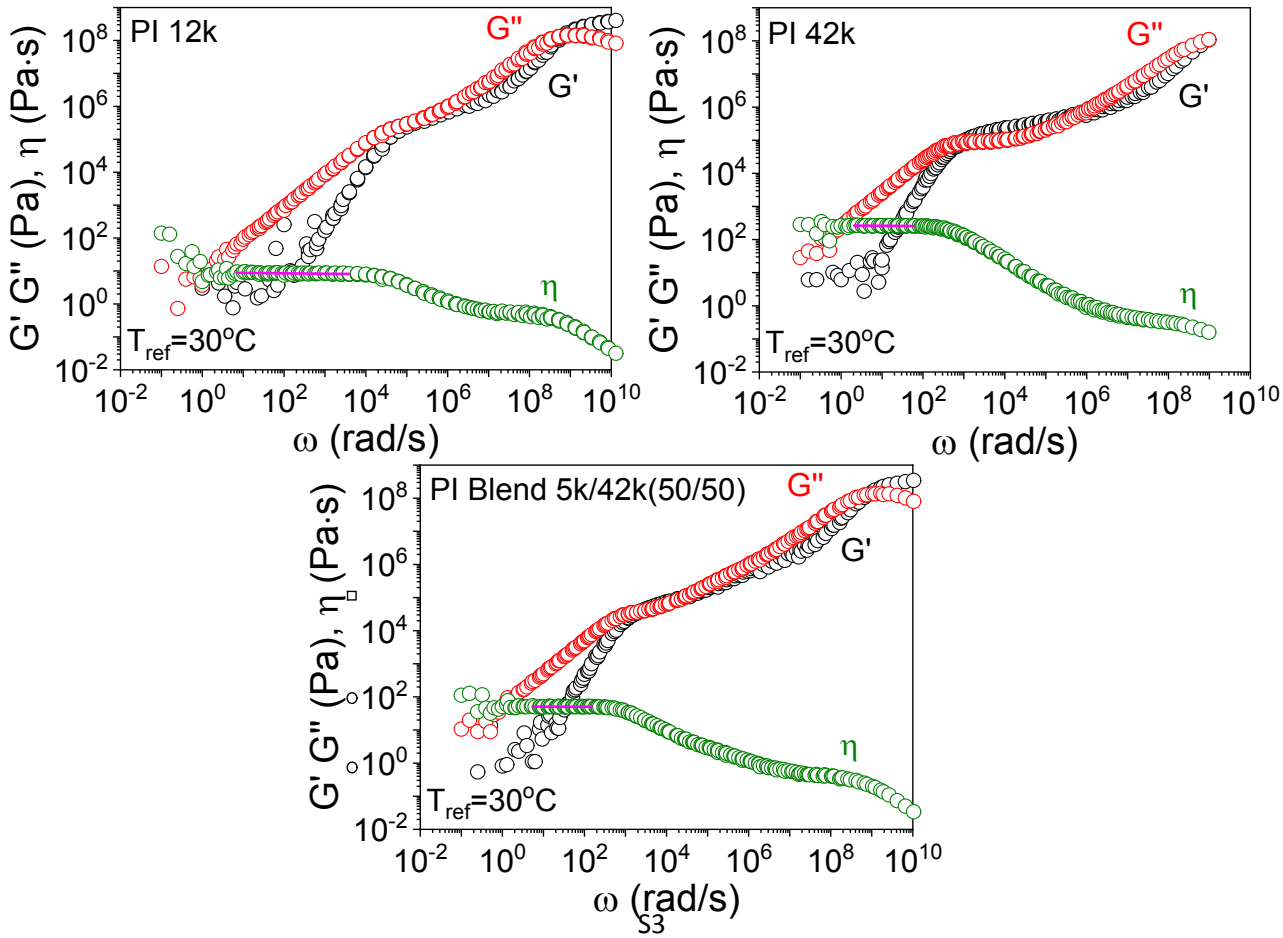

Figure S3. Master curves for the storage (black), the loss (red) moduli and the shear viscosity (green) all constructed at the same reference temperature (303.15 K).

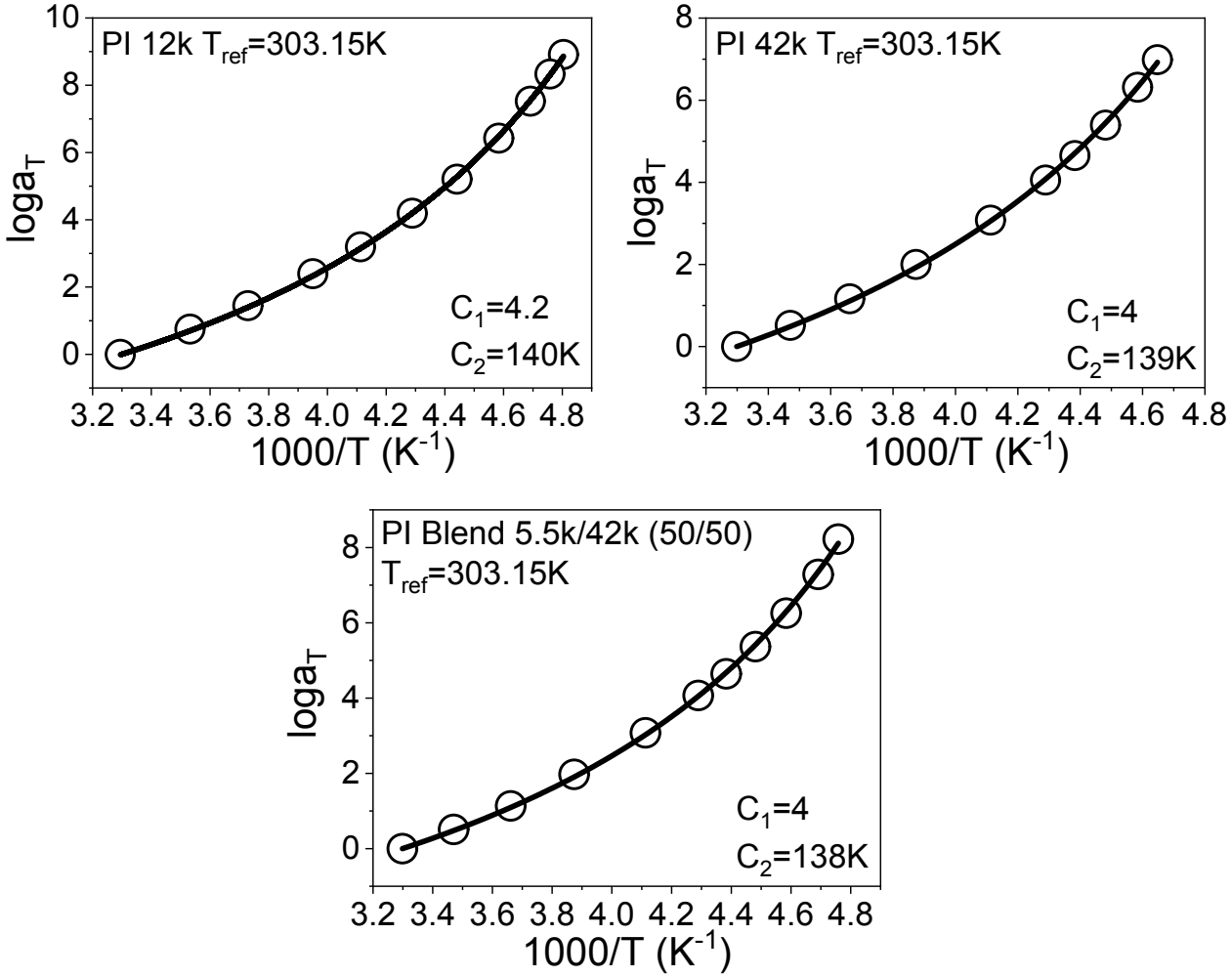

Figure S4. Shift factors for the homopolymers and the symmetric blend 5k/42k at the reference temperature (303.15 K). Solid lines represent fits to the WLF equation.

IV. Evolution of longest normal mode during and after imbibition

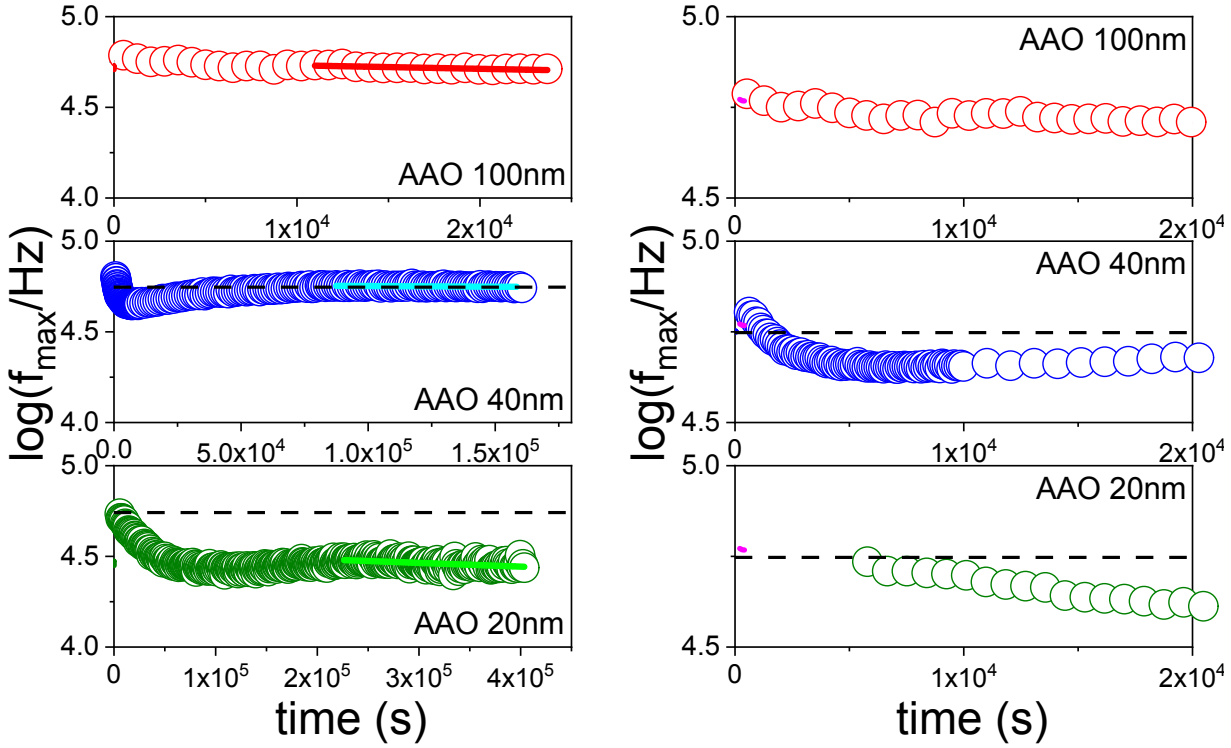

Figure S5. Evolution of peak position $\log(f_{max}/\mathrm{Hz})$ of the longest normal mode of **PI 5k** during in situ imbibition and adsorption process within different AAO templates with pore diameters (100 nm, 40 nm, and 20 nm): (left) entire imbibition and adsorption process and (right) zoom-in at the early stages. Black dashed lines indicate the frequency of the longest normal mode for the bulk polymer. Solid colored lines give the frequency of the peak position corresponding to the longest normal mode at the late stages. Notice the slower normal mode relaxation within the 20 nm pores as compared to the bulk.

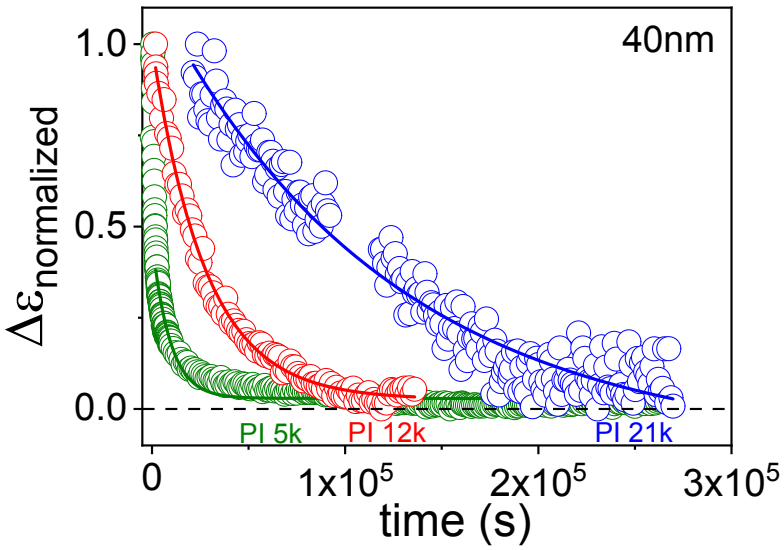

Figure S6. Evolution of dielectric intensity ($\Delta\varepsilon$) of **PI** with different molar masses during the *in situ* imbibition (and subsequent adsorption) within AAO nanopores with diameter of 40 nm at a temperature 303.15 K. Lines represent fits to an exponential decay function.

V. Polymer dynamics following imbibition

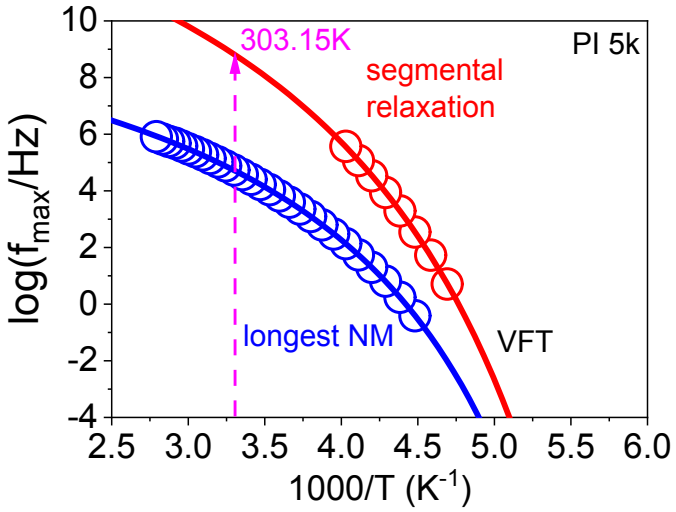

Figure S7. Arrhenius plot of the characteristic peak frequencies of **PI 5k**: longest normal mode (blue) and segmental relaxation (red). Solid lines are fits to the Vogel-Fulcher-Tammann equation. The vertical dashed line at 303.15 K indicates the peak frequencies of the normal mode and of the (extrapolated) segmental mode at the imbibition temperature.